Lithuanian Journal of Physics, Vol. **46**, No. 4, pp. 459–467 (2006) doi:10.3952/lithjphys.46409

SPIN CONDUCTANCE OF THE QUANTUM WIRE

A. Dargys

Semiconductor Physics Institute, A. Goštauto 11, LT-01108 Vilnius, Lithuania
E-mail: dargys@pfi.lt

Received 11 September 2006

The electron spin transport along a semiconducting quantum wire connected to spin-unpolarized electron reservoirs and the spin filtering properties of the wire are investigated. The wire is immersed in a magnetic field that is perpendicular to the wire axis and substrate plane on which the wire is grown. The lateral confining potential is assumed to be parabolic. The spin–orbit interaction is included via Rashba Hamiltonian that in conjunction with the Zeeman Hamiltonian determines the spin conductance of the wire. Dependences of the spin current and conductance on the voltage applied over the ends of the wire as well as on the magnetic field strength are analysed.

Keywords: quantum wire, spin transport, spin conductance

PACS: 73.21.La, 73.63.Nm, 85.35.Be, 85.75.-d, 67.57.Lm

1. Introduction

The controllable manipulation of electron and hole spins by electric and magnetic fields is a central theme in spintronics. One way to achieve this is via an intrinsic spin–orbit interaction in semiconductors. Two types of spin–orbit interaction are known in the literature. The first arises in *bulk* semiconductor compounds which do not have inversion symmetry [1]. The second arises in heterostructures that lack *structural* inversion symmetry [2, 3]. An important property of new semiconducting nanodevices related to structural asymmetry is the possibility to manipulate the strength of the asymmetry (or Rashba interaction) by external voltages as demonstrated experimentally in Refs. [4, 5].

In this article the spin filtering properties of the quantum wire (QWR) that lacks structural inversion symmetry is studied. The wire is assumed to be connected to two unpolarized reservoirs kept at thermal equilibrium but at unequal chemical potentials. When the Rashba and Zeeman Hamiltonians are included, the electrical current between the reservoirs appears to be spin polarized due to spin filtering in the quantum wire. In this article the properties of the spin current which is proportional to voltage are investigated as functions of the externally applied voltage and magnetic field in the nanowire.

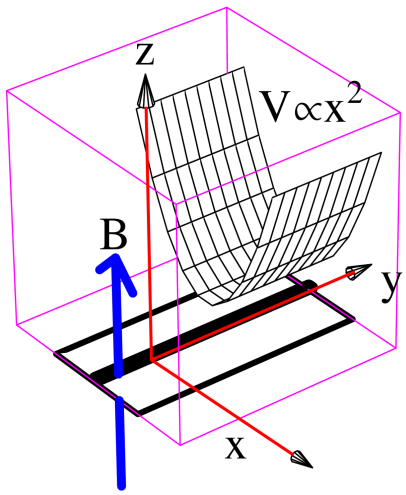

Fig. 1. Model of the quantum wire. The wire (thick central line) on xy plane is defined by two split gates (outer rectangles along the wire) on the 2D electron gas surface. The magnetic field **B** is perpendicular to the plane. The confining potential that forms the wire in y direction is proportional to x^2. The voltage between the ends of the wire is applied via 2D pads (not shown) that make an integral part of the film with 2D gas.

2. QWR model

We shall assume that the quantum wire has been formed on a two-dimensional (2D) film filled with 2D electron gas. The wire on the film can be defined by two

ISSN 1648-8504

gates on both sides of the wire, Fig. 1. The Hamiltonian that describes the behaviour of noninteracting electrons in the wire reads:

$$H = \frac{(\mathbf{p} + e\mathbf{A})^2}{2m^*} + V(x) + V(z) + H_{\rm Z} + H_{\rm R}$$
$$\equiv H_0 + H_{\rm R}\,, \qquad (1)$$

where $\mathbf{p} = (p_x, p_y, p_z)$ is the linear momentum, with components p_x and p_y being in the film plane, and m^* is the effective electron mass. The magnetic induction **B** is assumed to be directed along the z axis. **B** is present in the Zeeman Hamiltonian $H_{\rm Z}$ and in the kinetic term. In the latter it is described by the vector potential in the Landau gauge $\mathbf{A} = (0, Bx, 0)$, where $B = |\mathbf{B}|$. The electron can freely propagate only in y direction, Fig. 1. The voltage between the split gates is assumed to induce a parabolic lateral confining potential $V(x)$ in the x direction,

$$V(x) = \frac{m^*\omega_0^2 x^2}{2}\,, \qquad (2)$$

where ω_0 is an oscillator frequency. The triangular, or close to triangular potential $V(z)$ between the substrate and the film with 2D electron gas is assumed to be strong enough, so that only the lowest energy level related to $V(z)$ is occupied by electrons. In the following the total electron energy will be referenced relative to this lowest energy level. By this reason the dependence on z coordinate in the Hamiltonian (1) can be neglected altogether.

Apart from the kinetic term, the spin controlling properties in the Hamiltonian (1) also enter via the Zeeman $H_{\rm Z}$ and Rashba $H_{\rm R}$ terms. The Zeeman spin splitting Hamiltonian is

$$H_{\rm Z} = \frac{1}{2}\, g^* \mu_B B \sigma_z\,, \qquad (3)$$

where g^* is the effective magnetic factor (effective Landé g factor) and $\mu_{\rm B}$ is the Bohr magneton, $\mu_{\rm B} = e\hbar/2m_0$, with bare electron mass m_0. For electrons $g^* = -0.44$ in GaAs, $g^* = -1.9$ in InP, $g^* = -7.8$ in GaSb, $g^* = -15$ in InAs, $g^* = -51$ in InSb. The spin quantization axis is thought to be aligned along **B** as indicated by diagonal Pauli matrix σ_z. The Rashba Hamiltonian [2], the origin of which is related to the structural asymmetry in z direction, is

$$H_{\rm R} = \frac{\alpha}{\hbar}\left[\sigma_x(p_y + eBx) - \sigma_y p_x\right]. \qquad (4)$$

Here α is the Rashba constant. As concerns the spin–orbit interaction, apart from the Rashba there is also a bulk-related contribution [1]. The latter is also called the Dresselhaus contribution and is associated with the absence of an inversion symmetry in a compound, for example a zinc-blende-type semiconductor. The Rashba contribution usually dominates in narrow-gap materials and nanostructures considered here.

The Schrödinger equation with the Hamiltonian (1) is separable in x and y coordinates, so that its solution can be factorized in the following way:

$$\Psi(x, y) = \psi(x)\, \exp(\mathrm{i}k_y y)\,. \qquad (5)$$

Here $\psi(x)$ is the transverse part of the wave function and the exponent describes the running waves with the wave vectors k_y along the wire. Substitution of (5) into the unperturbed part H_0 of (1) gives one-dimensional Hamiltonian of the shifted harmonic oscillator plus a constant (independent of x) term:

$$H_0 = -\frac{\hbar^2}{2m^*}\frac{\mathrm{d}^2}{\mathrm{d}x^2} + \frac{m^*\omega^2}{2}(x - x_0)^2 + \frac{\omega_0^2}{\omega^2}\frac{\hbar^2 k_y^2}{2m^*}$$
$$+ \frac{1}{2} g \mu_{\rm B} B \sigma_z\,, \qquad (6)$$

where $\omega = \sqrt{\omega_0^2 + \omega_{\rm c}^2}$ is the effective oscillator frequency. The shift is $x_0 = (1 + \omega_0^2/\omega_{\rm c}^2)^{-2}(\hbar k_y/eB)$, where $\omega_{\rm c}$ is the cyclotron frequency, $\omega_{\rm c} = eB/m^*$. The shift is due to magnetic field. It vanishes when $B \to 0$. The solution of the unperturbed Hamiltonian (6) is given by [6]

$$\psi_{n\nu}^{(0)}(x) = \left(\frac{m^*\omega}{\pi\hbar}\right)^{1/4} \frac{\mathrm{e}^{-m^*\omega(x-x_0)^2/2\hbar}}{\sqrt{2^n n!}}$$
$$\times H_n\left((x - x_0)\sqrt{\frac{m^*\omega}{\hbar}}\right)\chi_\nu\,. \qquad (7)$$

In (7), $H_n(\xi)$ is the Hermite polynomial of the order $n = 0, 1, 2, \ldots$ and χ_ν is the spin eigenstate with the spin projection ν on the z axis, $\chi_\uparrow = \begin{pmatrix} 1 \\ 0 \end{pmatrix}$ and $\chi_\downarrow = \begin{pmatrix} 0 \\ 1 \end{pmatrix}$. The corresponding energy eigenvalues are given by

$$E_{n\uparrow,\downarrow}^{(0)} = \hbar\omega\left(a_n^\dagger a_n + \frac{1}{2}\right) + \frac{\omega_0^2}{\omega^2}\frac{\hbar^2 k_y^2}{2m^*} \pm \frac{1}{2} g \mu_{\rm B} B\,, \qquad (8)$$

where $a_n^\dagger$ and a_n are the standard raising and lowering operators, $a_n^\dagger a_n$ is the number operator with the eigenvalues $n = 0, 1, 2, \ldots$, and $\pm$ signs correspond to up and down spins with respect to **B**. The first term in (8) describes the discrete oscillator energies, the second term shows that every discrete level is associated with

a parabolic band, and the last term indicates that in the magnetic field the parabolic bands are split for the up and down spin states. The coefficient at k_y^2 shows that in the subband dispersion, in fact, the effective mass m^* has been replaced by $m^*(1+\omega_c^2/\omega_0^2)$, i. e. the effect of the magnetic field is to increase the effective mass of the electron that propagates along the wire. As a result, at high magnetic fields as we shall see the bands become flat.

The Hamiltonian H_0 with the Rashba term H_R neglected and the corresponding basis (6) will serve as a starting point in finding the dispersion and spin properties of the full Hamiltonian (1). The investigation shows that it is possible to obtain a good quantitive description of the lower energy bands of the wire if the truncated Hilbert space characterized by a finite oscillator number n is used [7, 8, 9, 10]. This is so because at $n \neq n'$ and in the basis $\chi_{\uparrow,\downarrow}$ the matrix elements $\langle\psi_{n\nu}(x)|H_R|\psi_{n'\nu'}(x)\rangle$ of the Rashba Hamiltonian

$$H_R = \alpha \begin{pmatrix} 0 & k_y + B\sqrt{\dfrac{\hbar}{2m^*\omega}}A_+ + \sqrt{\dfrac{\hbar m^*\omega}{2}}A_- \\ k_y + B\sqrt{\dfrac{\hbar}{2m^*\omega}}A_+ - \sqrt{\dfrac{\hbar m^*\omega}{2}}A_- & 0 \end{pmatrix}, \tag{9}$$

where $A_\pm = a \pm a^\dagger$ couple only the adjacent energy bands (8), i. e., due to properties of the lowering and raising operators one has $\langle\psi_m|a|\psi_n\rangle = \delta_{m,n-1}\sqrt{n}$ and $\langle\psi_m|a^\dagger|\psi_n\rangle = \delta_{m,n+1}\sqrt{n+1}$. Thus, when the quantum numbers n and m are large enough the truncation error in the highly excited states will reduce to negligibly small error for the ground and low-lying energy states. The neighbouring oscillator levels $n \pm 1$ will be coupled only if the unperturbed spinors possess oppositely directed spins in the matrix element $\langle n, \nu|H_R|n \pm 1, \nu'\rangle$, where $|n, \nu\rangle \equiv \psi^{(0)}_{n\nu}(x)$. Apart from $m = n \pm 1$ perturbation terms, there also appear $m = n$ terms that couple the opposite spins, too. This perturbation on the diagonal matrix elements is related to the wave vector k_y and is given by $\langle n, \uparrow |H_R|n, \downarrow\rangle = \alpha(1 - \omega_c^2/\omega^2)k_y$. The appearance of the cyclotron frequency in this expression comes from x_0.

Combining the diagonal part given by (8) and the coupling elements $\langle n, \nu|H_R|m, \nu'\rangle$, a large matrix was constructed which was then diagonalized or used to find the exact eigenfunctions numerically. Since the spin in the diagonalized in this way Hamiltonian is not a good quantum number, in the following the exact eigenfunctions ψ_l that correspond to energy bands l will be numbered by their increasing eigenvalues (energies) $l = 1, 2, \ldots$ rather than by their oscillator and mixed spin numbers. In the numerical calculations and analysis it is convenient to introduce the following characteristic lengths related to the oscillator ω_0 and cyclotron $\omega_c = eB/m^*$ frequencies and to the Rashba constant α:

$$L_0 = \sqrt{\frac{\hbar}{m^*\omega_0}}, \quad L_Z = \sqrt{\frac{\hbar}{m^*\omega_c}}, \quad L_R = \frac{\hbar^2}{2m^*\alpha}. \tag{10}$$

The oscillator length L_0 gives a characteristic spreading of the electron wave function in the transverse direction. The magnetic length L_Z is equal to the radius of the skipping electron trajectory along the wire at electron energy $\hbar\omega_c/2$ [11]. For parameters of InAs ($m^*/m_0 = 0.04$, $\alpha = 10^{-11}$ eV m, $g^* = -8$) at $L_0 = 31$ nm and $B = 1$ T one has $L_Z = 25.6$ nm and $L_R = 95$ nm.

Figure 2 shows the spectrum of the QWR at three characteristic strengths of the magnetic field. Here and in all subsequent figures the energy is measured in units of $\hbar\omega_0$ and the wave vectors in units of L_0^{-1}. For InAs at $L_0 = 31$ nm one has $\hbar\omega_0 = 2$ meV. At high magnetic field the bands are flat (Fig. 2(a)) and the adjacent energy levels carry opposite spins, the directions of which are either parallel or antiparallel to **B**. This can also be seen in Fig. 3, where the average spin Cartesian components of the two lowest bands are plotted as functions of the wave vector. It is seen that $\langle\sigma_z\rangle$ component predominates and has opposite signs in Fig. 3(a b). At high magnetic fields the influence of band mixing due to Rashba term (9) is small and the spectrum is described mainly by the first and the last terms in the dispersion (8). At intermediate magnetic fields the flattening effect of **B** becomes smaller and, as a result, in (8) the quadratic in k_y term makes the dispersion closer to parabolic as seen in Fig. 2(b). The bands still remain spin-split along the vertical axis by the Zeeman term, although the average spins now are not in pure states (compare with Fig. 5). In weak and zero magnetic fields the Rashba term prevails, what causes the bands with opposite spins to split along the horizontal axis, i. e. along the wave vector axis. At higher energies, as seen in Fig. 2(c), the band crossing takes place in this case.

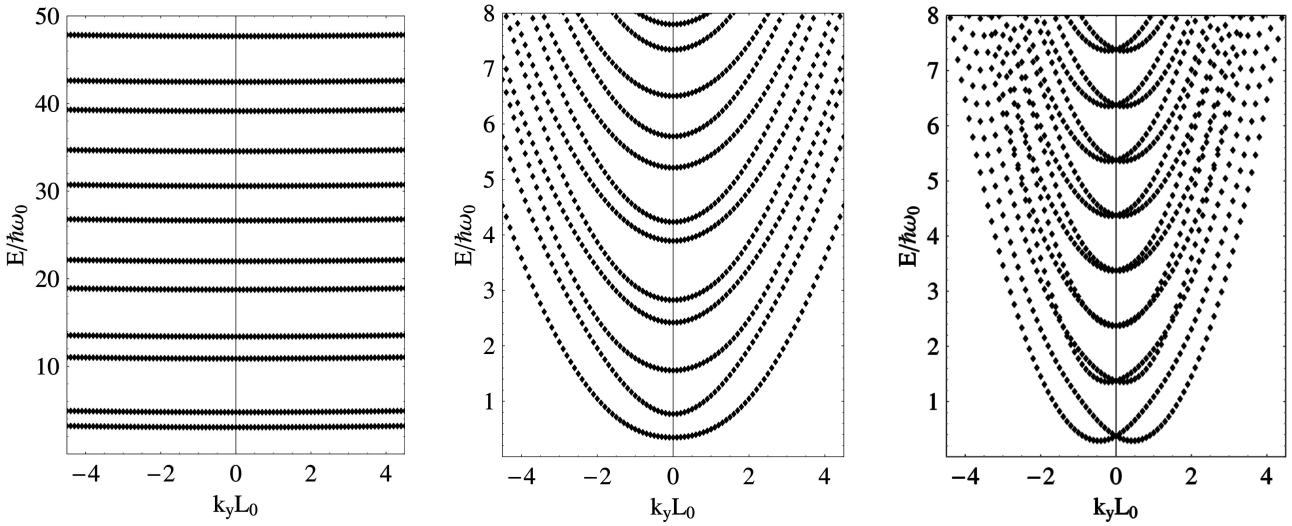

Fig. 2. The characteristic spectra of the wire at three magnetic field strengths: (a) high magnetic field, $L_{\rm Z} = 0.35$, (b) intermediate, $L_{\rm Z} = 1$, and (c) zero magnetic field, $L_{\rm Z} \to \infty$. The energy is normalized by the oscillator energy $\hbar\omega_0$ and the wave vector by transverse oscillator length L_0. The other parameters are $L_0 = 1$, $L_{\rm R} = 1$.

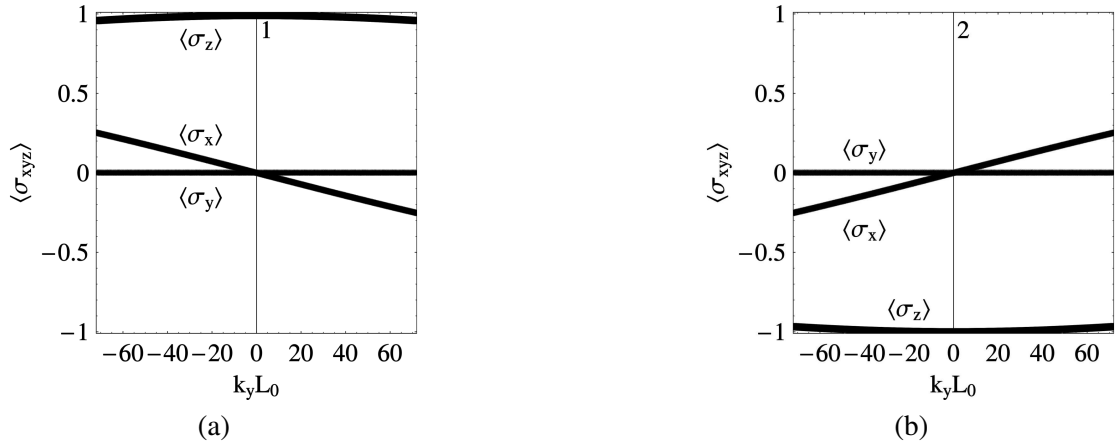

Fig. 3. Average spin components versus wave vector for the (a) ground and (b) first excited energy bands at high magnetic field. For respective pairs of bands at higher energies the dependencies have similar character. $L_{\rm R}/L_0 = 3$, $L_{\rm Z}/L_0 = 0.35$.

3. Spin transport

3.1. Spin conductivity

The spin current will be defined as the transportation of electron spin in a real space, when the average spin direction during movement along the wire remains unchanged. Thus, for an electron occupying a single energy band, the spin current related to spin projection $i = x$, y, or z can be written as

$$I_i^s = \frac{d\langle s_i\rangle}{dt} = \frac{\hbar}{2}\int\limits_{-\infty}^{\infty} \langle\nu|\sigma_i|\nu\rangle v_\nu(k) f_\nu(k)\,{\rm d}k\,, \quad (11)$$

where $\langle\nu|\sigma_i|\nu\rangle$ is the average spin in the eigenstate $|\nu\rangle$ that must be found from the wire Hamiltonian, $v_\nu(k)$ is the electron velocity along the wire at the wave vector k, and $f_\nu(k)$ is the distribution function. The factor $\hbar/2$ comes from the relation $s_i = \hbar\sigma_i/2$ between the spin s_i and Pauli σ_i matrices. As mentioned, it is supposed that during electron movement from one to other reservoir the spin does not change with time, otherwise a more refined definition of the spin current is required [12]. If 1D channel supports only those injected electrons that move in the positive direction, then the lower limit in the integral (11) is zero, i. e. $k = k_y = 0$ for the considered energy band. If, in addition, the temperature is low enough so that the electron concentration is zero at

energies $E > E_{\rm F}$, where $E_{\rm F}$ is the Fermi energy, then the spin current reduces to

$$I_i^s = \frac{\hbar}{2}\int_0^{E_{\rm F}} \langle\nu|\sigma_i|\nu\rangle v_\nu(E) f_\nu(E) N_\nu(E)\,{\rm d}E\,, \qquad (12)$$

where $N_\nu(E)$ is the density of states. For a parabolic dispersion law, $E = \hbar^2k^2/2m^*$, the electron velocity is $v = \partial E/\partial(\hbar k) = \hbar k/m^*$. Then the corresponding density of states becomes

$$N(E) = \sqrt{\frac{m^*}{2\pi\hbar E}} = \frac{1}{\pi\hbar v}\,. \qquad (13)$$

Remembering that at zero temperature $f_\nu(E) = 1$ when the energy E is below the Fermi energy $E_{\rm F}$, the equation (12) can be reduced to

$$I_i^s = \frac{1}{2\pi}\int_0^{E_{\rm F}} \langle\nu|\sigma_i|\nu\rangle\,{\rm d}E\,, \qquad (14)$$

where the well-known cancellation of the velocity and density of states was used. When the electron is in a pure spin state, for example, aligned with the z axis, the eigenstates in (14) are $|\nu\rangle = \begin{pmatrix}1\\0\end{pmatrix}$ or $|\nu\rangle = \begin{pmatrix}0\\1\end{pmatrix}$. However, in general case, when a universal quantization axis cannot be defined, the average spin $\langle\sigma_i\rangle = \langle\nu|\sigma_i|\nu\rangle$ depends on the wave vector k and, therefore, on electron energy E. The energy interval 0–$E_{\rm F}$ in the integral (14) can be expressed as a difference between the electrochemical potentials μ_1 and μ_2 in left and right electron reservoirs connected to 1D conductor: $E_{\rm F} = \mu_1 - \mu_2 = -eV$, where V is the voltage applied between the reservoirs. In accordance with the arguments of Landauer, Büttiker, and Imry [13–15], it is assumed that there is no potential drop in the channel. The potential drop that is associated with a finite resistance occurs at the connections to the reservoirs, and V is supposedly divided equally between the two tapered connectors. This is essential, since the conduction can be calculated after specifying the location where the potential drop occurs [15]. The integral in (14) can be evaluated if the dependence of spin on the wave vector magnitude and direction is known. For continuous functions, according to the mean value theorem [16], the integral can be written as $e\langle\nu(\mu)|\sigma_i|\nu(\mu)\rangle V$, where μ is the energy in the interval μ_1–μ_2. Since the wire acts as a spin filter that allows the propagation of electronic waves having a well-defined energy (related to k via the dispersion relation), we shall assume that $\mu = eV/2$. Then, the spin conductivity (or conductance, since it appears to be independent of sample dimensions) related to a single energy subband will be

$$G_i^s = \frac{I_i^s}{V} = \frac{e}{2\pi}\langle\nu(\mu)|\sigma_i|\nu(\mu)\rangle\,. \qquad (15)$$

In a pure spin state, $|\nu\rangle = \begin{pmatrix}1\\0\end{pmatrix}$ or $|\nu\rangle = \begin{pmatrix}0\\1\end{pmatrix}$, one has $\langle\nu(\mu)|\sigma_i|\nu(\mu)\rangle = \pm1$ or 0. In this case from (15) follows that an elementary spin conductance is $G_i^s = \pm e/2\pi$. If electron can propagate in two channels that support oppositely directed spins then the total spin current will be zero due to cancellation of spins. Thus, in pure states the total spin conductance will be zero either due to spin cancellation in adjacent channels that carry opposite spins, or when the spin is perpendicular to the quantization axis.

The obtained spin conductance (15) for a single channel (subband) can be generalized to multiband case. When one has n energy subbands, with the nth subband having j local extrema $\xi_n^{(j)}$, the total spin conductivity then becomes the sum over the subbands and extremal points

$$\mathcal{G}_i^s = \mathcal{G}_0^s \sum_{n,j} \langle\nu_n(\mu - \xi_n^{(j)})|\sigma_i|\nu_n(\mu - \xi_n^{(j)})\rangle$$

$$\times\Theta(\mu - \xi_n^{(j)})\,{\rm sgn}(m_n^{*(j)})\,, \qquad (16)$$

where $\mathcal{G}_0^s = e/(2\pi)$ and the signum function accounts for the type of the extremal point. It is positive for energy minimum and negative for energy maximum. The Heaviside Θ-function takes into account the open channels at a given applied voltage. The formula (16) is analogous to the quantized electrical conductance formula, therefore, its domain of applicability is similar, as discussed in Ref. [17]. Normally, with the increase of V the signs of spin projections in the "opened" bands alternate, and as a result, the spin conductance, in contrast to the electrical conductance, as we shall see, will have an alternating character. From the comparison of expression (16) with the analogous formula for quantized electrical conductance (see, for example, the book [11]) it can be concluded that the measurements of spin conductance may give more information on 1D band properties, since the average spin magnitude also depends on the applied voltage, whereas in the analogous formula for electrical conductance, instead of the average spin the constant (elementary charge) appears.

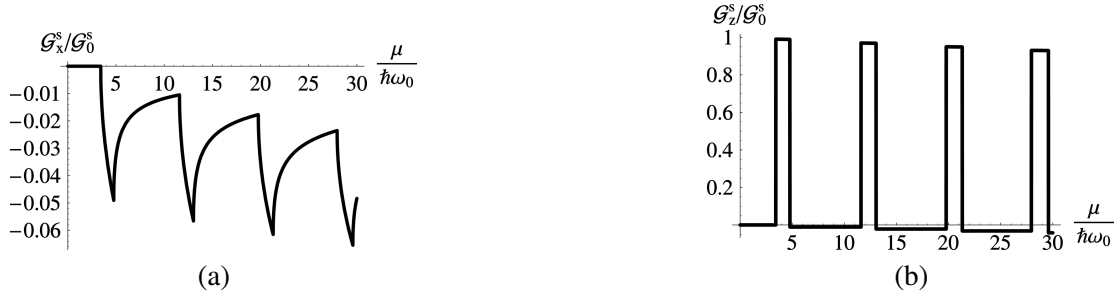

Fig. 4. The average (a) x and (b) z components of the normalized spin conductivity as functions of the normalized Fermi energy difference μ (or applied voltage) between the ends of the wire. $L_{\rm R}/L_0 = 3$, $L_{\rm Z}/L_0 = 0.35$.

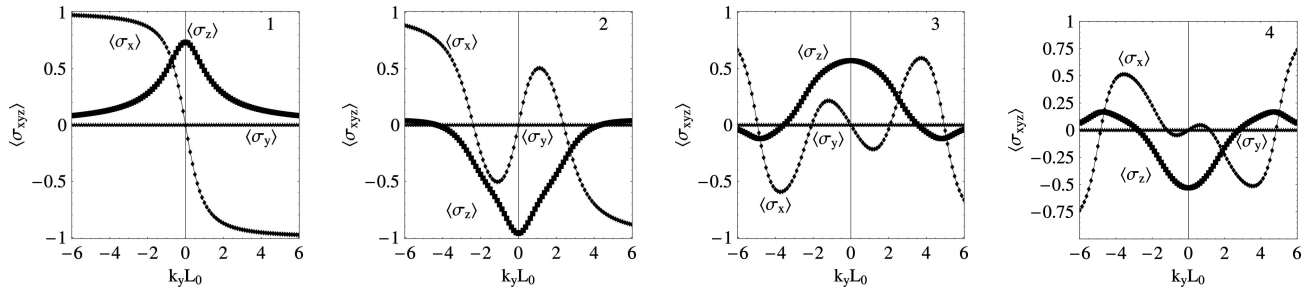

Fig. 5. Average spins versus wave vector at intermediate magnetic field for the four lowest subbands at $L_{\rm R}/L_0 = 1$, $L_{\rm Z}/L_0 = 1$. The numbers on the panels correspond to increasing subband energies (numbers).

3.2. Spin conductivity versus voltage at various magnitudes of B

As mentioned, at high magnetic fields the spectral and spin properties are determined mainly by Zeeman rather than Rashba Hamiltonian, as a result at high magnetic fields the spin is aligned along or against **B** direction. Figure 3 shows spin projections in two lowest energy subbands, which as can be seen from Fig. 2(a) are flat, i. e. nearly independent of k_y. The origin of the flatness, as explained earlier, comes from the unperturbed Hamiltonian (6). Similar picture was observed for higher energy bands. In agreement with the earlier investigations [7, 8, 9, 10], the electrical conductivity was found to increase in steps with the voltage amplitude. Appearance of a new step reflects the switching on of a new mode (conducting channel), where an extra electron can propagate along the wire. Since the total spin is equal to sum of individual spins of all open channels, while the adjacent channels carry opposite spins, the resulting spin conductance $\mathcal{G}^s_i$ consists of nearly equal amplitude pulses whose spins are parallel to z axis, Fig. 4. The pulse length is equal to energetic distance between two bands that carry opposite spins. The spin is equal zero when the number of bands that are open is even. As noted in Ref. [7], in the limit $B \to \infty$ the considered model converges to the exactly integrable Jaynes–Cummings model, one of the most simple models that couples the boson mode and a two-level system.

In Figs. 3 and 4 the ratio of characteristic lengths is $L_{\rm R}/L_0 = 3$, $L_{\rm Z}/L_0 = 0.35$. In InAs the Rashba length is $L_{\rm R} = 95$ nm, then, at the oscillator quantum $\hbar\omega_0 = 0.02$ meV (or $L_0 = 317$ nm, the length that roughly defines the current carrying strip width in Fig. 1) the magnetic induction is found to be $B = 0.054$ T. If the characteristic oscillator length is decreased to $L_0 = 31.7$ nm ($\hbar\omega_0 = 2$ meV) then $B = 5.4$ T.

The average spin component along the wire axis in all cases was found to vanish, i. e. $\langle\sigma_y\rangle = 0$. This is seen in Figs. 3 and 4 and in all subsequent figures. This means that independent of the wave vector the total electron spin is perpendicular to the wire axis. This property is associated with the symmetry of the Hamiltonian, which in our case is real and symmetric. The eigenvalues of such Hamiltonian are real too, what implies zero y component of the spin.

At intermediate magnetic fields the spectrum and spin properties are determined by both Rashba and Zeeman Hamiltonians. The spectrum in this case appears to be more or less parabolic, Fig. 2(b). The spin components $\langle\sigma_x\rangle$ and $\langle\sigma_z\rangle$ on average are of a comparable magnitude as can be seen from Fig. 5. Since at $k_y = 0$ the Rashba term (4) vanishes, the spin is directed along

Fig. 6. Dependence of x and z components of the normalized spin conductivity on the Fermi energy difference between the ends of the wire at intermediate magnetic field. $L_R/L_0 = 1$, $L_Z/L_0 = 1$.

Fig. 7. (a) Dependence of z component of the normalized spin conductivity on the Fermi energy difference at intermediate magnetic field which is 4 times weaker than in Fig. 6. The panel (b) shows contributions of the first eight channels to the total spin in the panel (a). $L_R/L_0 = 1$, $L_Z/L_0 = 2$.

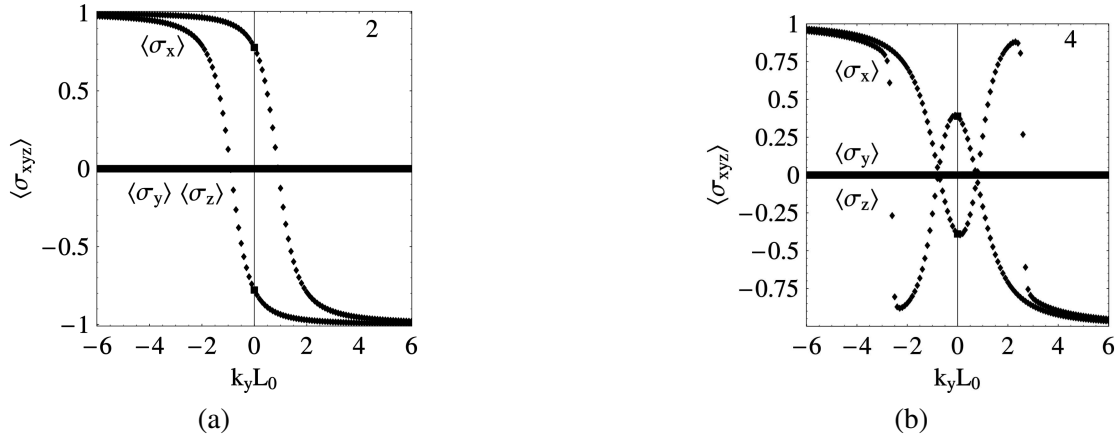

Fig. 8. Average spin projections versus wave vector at magnetic field close to zero. To emphasize the symmetry, the pairs of spins of the adjacent bands, panels *1–2* in (a) and panels *3–4* in (b), are plotted on the same panel. $L_R/L_0 = 1$, $L_Z/L_0 = 1000$.

magnetic field, i. e. along z axis for all subbands near the point $k_y = 0$. At larger wave vectors the oscillations of the spin projections are associated with the oscillations of the excited wave functions of the shifted oscillator. The variation of spin projections with k_y in Fig. 5 is also mirrored in the spin dependence on the applied voltage, Fig. 6. The component $\langle\sigma_z\rangle$ still has a pulsed character, with the abrupt changes of the spin magnitude at the crossings of the Fermi level with next higher energy subband minima, whereas $\langle\sigma_x\rangle$ component, due to contribution of the adjacent bands (channels), does not reduce to zero and even may be larger than that for a single channel. Thus, the compensation of the total spin after switching on of a new subband in this case is not complete. This reflects the property that under the action of Zeeman and Rashba Hamiltonians the spin is not in one of the pure up- or down-spin states $\chi_{\uparrow,\downarrow}$ and the average spin in different bands changes in a different manner versus k_y, Fig. 5. From this follows that the measurement of the spin current or conductance as a function of the voltage applied between the reservoirs may give new information on the

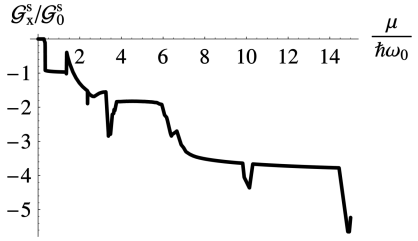

Fig. 9. Dependence of the x component of the normalized spin conductivity on the Fermi energy difference. The z spin component $\mathcal{G}_z^s$ is zero in this case. $L_{\rm R}/L_0 = 1$, $L_{\rm Z}/L_0 = 1000$.

properties of 1D system. Recently there was proposed a method how to determine the spins of charge carriers transported in wires [18]. In the method a pair of closely spaced point contacts were used to measure the spin polarization of valence band holes. The holes were injected from the end of one wire and collected by the other, adjacent wire. The spin polarization as high as 40% was detected with this system.

Figure 7 illustrates the z component of spin conductance versus wave vector along with the contribution by various channels (panel (b)) to the total conductance at the intermediate magnetic field, which is fourfold weaker than in Fig. 6. Since at $k_y = 0$ the z component is the largest (cf. Fig. 5), the opening of the nth channel is accompanied by the appearance of a new term $\langle\sigma_z\rangle_n$ and a peak in the total spin conductance. In contrast, the x component of the total spin conductance is found to be continuous (see, for example, the panel (a) in Fig. 5), since at $k_y = 0$ the Rashba term is ineffective and as a result $\langle\sigma_x\rangle_n = 0$ when $k_y = 0$.

Finally, at zero (or close to zero) magnetic field the Rashba interaction prevails, Figs. 8 and 9. The spin-splitting of the energy bands in this case is along horizontal axis rather than along vertical (energy) axis as seen in Fig. 2(c). The splitting is the larger the larger Rashba constant α is. In the absence of a magnetic field one finds $\langle\sigma_y\rangle_n = \langle\sigma_z\rangle_n = 0$, and as a result, after the switching on of a new channel the x component of the total spin suffers a discontinuity and the total spin remains parallel to x axis for all values of the voltage over the wire.

4. Summary and conclusions

Spectrum, wave functions, and transport of spin along the quantum wire connected to two unpolarized electron reservoirs at zero temperature were analysed. The Rashba interaction, which is due to wire structural asymmetry, and the Zeeman interaction determine the injected from the reservoir spin properties in the conducting channel. These two mechanism fix the electron spin in the plane perpendicular to the wire axis. The transport properties in the states where the electron has a well-defined energy in the occupied subband was considered only. The interference between closely lying channels was neglected. Due to mixing between Zeeman and Rashba Hamiltonians, the resulting spin of individual channels depends on the oscillator quantum number and electron propagation wave vector. As a result, the total spin current along the wire (or equivalently the spin conductance) was found to be a complicated function of the applied external voltage. Only at high magnetic fields, when the Zeeman term dominates and the spin is in a pure $\pm\hbar/2$ state, the total transferred between the reservoirs spin acquires a toothed structure with teeth amplitude $\hbar/2$ as the voltage is increased. In general, due to Rashba and Zeeman interaction, spin projections are in mixed states. This is reflected in the spin transport, which in its turn may be used to extract spin-related physical properties of the wire.

The standard methods of finding the electron spectrum in nanostructures are based on measurement of the quantized conductance or quantized Hall voltage as a function of bias or magnetic field [11]. The above discussed spin filtering properties of the quantum wire can also be adapted to determine the spectrum of nanostructures. This was recently demonstrated using the pairs of quantum wires subjected to external magnetic field [18, 19]. In addition, it should be noted that the quantum wire that carries the uncompensated electronic spin at the same is magnetized. Measurement of the magnetization of the wire with the help of small stripes of magnetic material deposited across the wire also may give useful information on the spectrum and magnetic properties of the wire. Alternatively, the integrated micromechanical magnetometer may be used for this purpose as demonstrated recently for 2D electron gas [20].

References

[1] G. Dresselhaus, Spin–orbit coupling effects in zinc-blende structures, Phys. Rev. **100**(2), 580–586 (1955).

[2] Y.A. Bychkov and E.I. Rashba, Properties of 2D electron gas with the lifted degeneracy in spectrum, Pis'ma Zh. Eksp. Teor. Fiz. [JETP Lett.] **39**(2), 66–69 (1964).

[3] Y.A. Bychkov and E.I. Rashba, Oscillatory effects and the magnetic susceptibility of carriers in inversion layers, J. Phys. C **17**(33), 6039–6045 (1984).

[4] G. Engels, J. Lange, T. Schäpers, and H. Lüth, Experimental and theoretical approach to spin splitting in modulation doped $In_xGa_{1-x}As$ / InP quantum well for $B \to 0$, Phys. Rev. B **55**(4), R1958–R1961 (1997).

[5] D. Grundler, Large Rashba splitting in InAs quantum wells due to electron wave function penetration into the barrier layers, Phys. Rev. Lett. **84**(26), 6074–6077 (2000).
[6] L.V. Landau and E.M. Lifshits, *Quantum Mechanics* (Nauka, Moscow, 1974), Ch. 3 and 15 [in Russian].
[7] S. Debald and B. Kramer, Rashba effect and magnetic field in semiconductor quantum wires, Phys. Rev. B **71**(11), 115322-1–6 (2005).
[8] J. Knobbe and T. Schäpers, Magnetosubbands of semiconductor quantum wires with Rashba spin–orbit coupling, Phys. Rev. B **71**(3), 035311-1–6 (2005).
[9] S. Zhang, R. Liang, E. Zhang, L. Zhang, and Y. Liu, Magnetosubbands of semiconductor quantum wires with Rashba and Dresselhaus spin–orbit coupling, Phys. Rev. B **73**(15), 155316-1–7 (2006).
[10] S. Bellucci and P. Onorato, Rashba effect in 2D mesoscopic systems with transverse magnetic field, `arXiv:cond-mat/0311051`, 1–12 (2003).
[11] S. Datta, *Electronic Transport in Mesoscopic Systems* (Cambridge University Press, New York, 1995).
[12] J. Shi, P. Zhang, D. Xiao, and Q. Niu, Proper definition of spin current in spin–orbit coupled systems, Phys. Rev. Lett. **96**(27), 076604-1–4 (2006).
[13] R. Landauer, Spatial variations of currents and fields due to localized scatterers in metallic conduction, IBM J. Res. Devel. **1**(3), 223–231 (1957).
[14] M. Büttiker, Symmetry and electrical conduction, IBM J. Res. Devel. **32**(3), 317–334 (1988).
[15] Y. Imry and R. Landauer, Conductance viewed as transmission, Rev. Mod. Phys. **71**(2), S306–S312 (1999).
[16] G.A. Korn and T.M. Korn, *Mathematical Handbook for Scientists and Engineers* (McGraw–Hill Book Company, New York, 1961), Ch. 4.
[17] A.V. Moroz and C.H.W. Barnes, Effect of the spin–orbit interaction on the band structure and conductance of quasi-one-dimensional systems, Phys. Rev. B **60**(20), 14272–14285 (1999).
[18] L.P. Rokhinson, V. Larkina, Y.B. Lyanda-Geller, L.N. Pfeiffer, and K.W. West, Spin separation in cyclotron motion, Phys. Rev. Lett. **93**(14), 146601-1–4 (2004).
[19] L.P. Rokhinson, L.N. Pfeiffer, and K.W. West, Spontaneous spin polarization in quantum point contacts, Phys. Rev. Lett. **96**(15), 156602-1–4 (2006).
[20] J.G.E. Harris, D.D. Awschalom, K.D. Maranowski, and A.C. Gossard, Magnetization and dissipation measurements in the quantum Hall regime using an integrated micromechanical magnetometer, J. Appl. Phys. **87**(9), 5102–5104 (2000).

KVANTINĖS VIELOS SUKININIS LAIDUMAS

A. Dargys

Puslaidininkių fizikos institutas, Vilnius, Lietuva

Santrauka

Išnagrinėta elektrono sukinio pernaša išilgai kvantinės vielos, kurios galai prijungti prie nepoliarizuotų elektronų rezervuarų, taip pat išnagrinėti kvantinės vielos sukinio filtravimo ypatumai. Sprendžiant uždavinį buvo padaryta prielaida, kad vielos plotį lemiantis potencialas turi parabolinį pavidalą, o magnetinis laukas yra statmenas vielos ašiai ir padėklui, ant kurio užauginta viela. Į sąveika tarp elektrono sukinio ir jo orbitinio judėjimo yra atsižvelgta per Rašbos (Rashba) pasiūlytą hamiltonianą, kuris kartu su Zėmano (Zeeman) hamiltonianu lemia sukinio srovės stiprį kvantinėje vieloje. Išnagrinėta sukinio srovės (laidumo) priklausomybė tiek nuo įtampos tarp kvantinės vielos galų, tiek nuo magnetinio lauko stiprio. Sukininio laidumo savybės straipsnyje pailiustruotos piešiniais.